Charge transfer in collisions of the effectively-one-electron isocharged ions Si^{3+}, C^{3+}, and O^{3+} with atomic hydrogen

N. L. Guevara, E. Teixeira, B. Hall, Y. Öhrn, E. Deumens, and J. R. Sabin
Quantum Theory Project, Departments of Physics and Chemistry, University of Florida, Gainesville, FL 32611-8435, USA
(Received 9 September 2010; revised manuscript received 13 January 2011; published 23 May 2011)

In a recent paper [Phys. Rev. A **77**, 064702 (2008)], Bruhns *et al.* reported on an experimental investigation of charge transfer in collisions of Si^{3+} ions with atomic hydrogen and compared the energy dependence of the transfer cross sections with published theoretical results and with earlier experimental results for other effectively-one-electron isocharged ions, including C^{3+} and O^{3+}. These authors observe that these three ions all have the structure of a single electron outside a closed subshell and thus might be expected to behave similarly. However, their results show quite different behavior, and they conclude that the influence of quantum-mechanical effects from the ionic core is clearly seen. We have investigated theoretically three collision systems, Si^{3+}, C^{3+}, and O^{3+} with atomic hydrogen, at projectile energies up to 10 keV/amu using the method of electron nuclear dynamics (END). In this paper we want to clarify and describe in some detail these quantum-mechanical effects by showing the time-dependent dynamics of the electrons during the collision of these three ions with atomic hydrogen. Total charge transfer cross sections were calculated for all three ions and compared with other theoretical and experimental results, showing good overall agreement. With this validation of the END description of the processes, we analyze the details of the computed dynamics of the electrons in each of the processes and illustrate the different mechanisms underlying observed differences in reaction outcomes.

DOI: 10.1103/PhysRevA.83.052709 PACS number(s): 34.10.+x, 34.70.+e

I. INTRODUCTION

In the past decades, electron capture by multiply charged ions from atomic hydrogen has been the subject of intensive experimental and theoretical work, mainly due to its important role in the composition of the interstellar medium [1]. It is thus important to develop and test theoretical models that can describe electron capture processes of this sort accurately.

Recently, Bruhns *et al.* [2] studied collisions of Si^{3+} with atomic hydrogen experimentally and made a comparison with the results from similar measurements on C^{3+} [3] and O^{3+} [4]. They also compared their Si^{3+} results with theoretical results [5] obtained with the classical-trajectory Monte Carlo (CTMC) and quantum-mechanical molecular-orbital close-coupling (MOCC) methods. As all three projectiles are effective one-electron systems with equal charges ($q = 3+$), one might expect similarities among the three collision systems. However, they found qualitative differences in the charge-transfer cross sections for the three projectiles. The largest difference was observed for the charge-transfer cross section for O^{3+} colliding with hydrogen. But even for the collision processes of C^{3+} and Si^{3+} on H the charge-transfer cross sections show a different energy dependence. The authors conclude that these differences stem from the influence of quantum-mechanical effects of the ionic core.

In the present work, the process of electron transfer in collisions of the effective one-electron isocharged ions Si^{3+}, C^{3+}, and O^{3+} on atomic hydrogen at energies between about 0.04 keV/amu and 10 keV/amu is investigated theoretically in an attempt to further understand the dynamical underpinnings of the differences observed.

Most of the theoretical work treating collisions of dressed ions having few electrons outside a closed shell or subshell with hydrogen atoms uses a parametric model potential to account for the effect of the core electrons [5–8]. This suitably allows the problem to be reduced to an effective one- or two-electron process. Some methods use a full quantum-mechanical treatment of the nuclear motion [5,6], others use a semiclassical treatment with straight-line trajectories for the nuclei [7,8].

The investigation in this paper is executed using electron nuclear dynamics (END) [9,10]. Previous work using the END formalism has shown [11] that proper coupling of electronic and nuclear motion is important to obtain qualitative and quantitative agreement with the experimental charge-transfer probabilities and differential cross sections for $H^+ + H$ collisions. It is thus expected that END can provide a reliable physical description of one-electron transfer collisions in the systems under consideration here.

After we establish that this method gives results in reasonable agreement with previous works, both experimental and theoretical, we analyze the details of the computations to extract information regarding the dynamics during the process to clarify and further explain the differences between the transfer processes. END is particularly suited for such study as it is a method that includes all electrons in the wave function, uses fully dynamical, easy-to-interpret semiclassical nuclear trajectories for the nuclei, and includes all interaction terms between electronic and nuclear degrees of freedom.

The paper is organized as follows. A brief overview of the theoretical and computational methods used is given in Sec. II. We analyze in detail the collision processes in the three cases with particular emphasis on what happens to the electronic wave function as a function of time during the collision in Sec. III. We formulate the summary of our findings in Sec. IV, providing more detailed insight on the observations made in earlier work.

II. THEORETICAL APPROACH

Electron nuclear dynamics is based on the application of the time-dependent variational principle (TDVP) to the Schrödinger equation, and describes the system wave function in a coherent state representation. Here, only a brief description

of the theory is given since END has been described in detail elsewhere [9,10].

A. Propagation of the wave function

The variational wave function is parameterized as a coherent state manifold [12,13] where the electronic and nuclear degrees of freedom are coupled. The END total wave function can be expressed as

$$|\Psi(t)\rangle = |z(t),\mathbf{R}(t),\mathbf{P}(t)\rangle|\mathbf{R}(t),\mathbf{P}(t)\rangle, \tag{1}$$

where $|z,\mathbf{R},\mathbf{P}\rangle$ and $|\mathbf{R},\mathbf{P}\rangle$ are the electronic and nuclear wave functions, respectively. Here $\mathbf{R}$ and $\mathbf{P}$ stand for the average position and momenta of all nuclei, and the z are time-dependent coefficients that describe the electron dynamics.

The electronic wave function is then expressed as a single, complex, spin-unrestricted Thouless determinant [14],

$$\Phi(\mathbf{x}) = \langle \mathbf{x}|z,\mathbf{R},\mathbf{P}\rangle = \det\{\chi_k(\mathbf{x}_l,z,\mathbf{R},\mathbf{P})\}, \tag{2}$$

where $\mathbf{x}_j$ are the space-spin coordinates of electron j. The determinantal wave function is built from nonorthogonal, dynamic spin orbitals,

$$\chi_i = \phi_i + \sum_{j=N+1}^{K} \phi_j\, z_{ji}, \qquad i = 1,2,\ldots,N \tag{3}$$

with ϕ_j a suitable basis of atomic orbitals. This representation takes into account the momentum of the electron explicitly through electron translation factors [15]. One should note that the molecular-orbital coefficients z_{ji} are complex. This electronic wave function is a particular representation of a so-called generalized coherent state [13]. The nuclear part of the wave function $\langle X|\mathbf{R}(t),\mathbf{P}(t)\rangle$ uses the narrow wave-packet limit for the traveling Gaussians, which leads to the nuclear trajectories being represented as classical trajectories $(\mathbf{R},\mathbf{P})$. This makes END results easier to interpret, but leaves the need to verify that the quantum interference effects between different nuclear trajectories can be neglected.

The time-dependent variational principle [12] is based on the variation of an action functional $A = \int_{t_1}^{t_2} L(\Psi^*,\Psi)\mathrm{d}t$ with the quantum-mechanical Lagrangian,

$$L(\Psi^*,\Psi) = \left[\frac{i}{2}(\langle\Psi|\dot{\Psi}\rangle - \langle\dot{\Psi}|\Psi\rangle) - \langle\Psi|\hat{\mathrm{H}}|\Psi\rangle\right]\langle\Psi|\Psi\rangle^{-1}, \tag{4}$$

generating the coupled Euler-Lagrange equations required for the dynamical evolution of the system including the complete dynamics of both electrons and nuclei. The dynamical variables are $(\mathbf{R},\mathbf{P},z,z^*)$, where $\mathbf{R}$ and $\mathbf{P}$ are the position and momentum of the nuclei and z and z^* are the Thouless coefficients and their complex conjugate. The solution of these equations of motion is implemented in the computer software ENDyne [16].

B. Analysis of final states

The initial wave function

$$\begin{aligned}\Phi_i(\mathbf{x}) &= \det\{\chi_k(\mathbf{x}_k,z(t_i),\mathbf{R}(t_i),\mathbf{P}(t_i))\}\\ &= \det\{\theta_k(\mathbf{x}_l)\}\end{aligned} \tag{5}$$

is obtained as the solution of the Hartree-Fock (HF) equations at the initial geometry $\mathbf{R}(t_i)$, which has the projectile far from the target. We typically place the target at the origin and let the projectile fly in along the negative z axis,

$$\mathbf{R}(t_i) = (b\mathbf{e}_x - d\mathbf{e}_z,\mathbf{0}), \tag{6}$$

where b is the impact parameter and $-d$ is the z coordinate of the projectile at the start of the simulation. Because the ions are far apart, this initial HF wave function is the product of the atomic HF for the projectile ion and the hydrogen.

The wave function is then propagated until time t_f, which is taken to be large enough so that there is no more interaction between the fragments of the collision, except possibly Coulomb interaction if some fragments are charged. We verify that the total charge of each fragment does not change anymore for times around t_f.

Then we analyze the wave function to determine charge-transfer and state-specific differential cross sections by computing the overlap of the evolved END wave function with suitable states that are products of wave functions for the fragments,

$$|\langle\Phi_{i\to f}|\Theta\rangle|^2. \tag{7}$$

For example, to compute the charge-transfer cross section we determine the wave function $P_I\Phi_{i\to f}(\mathbf{x})$ as the projection of $\Phi_{i\to f}(\mathbf{x})$ on the space of all wave functions with all electrons on the ion,

$$\Theta(\mathbf{x}) = \det\{\theta_k(\mathbf{x}_l)\}, \tag{8}$$

with the spin orbitals θ_k of the form

$$\theta_k(\mathbf{x}) = \sum_{j\in I} c_{kj}\phi_j(\mathbf{x}) \tag{9}$$

and with I the list of spin orbitals centered on the ion, excluding the spin orbitals centered on the hydrogen. Since the ions are far apart, there is no overlap between the spin orbitals on the different centers. Note that this projection can be a superposition of determinants and does not have to be a single determinant even when $\Phi_{i\to f}(\mathbf{x})$ is. The projection is carried out at the final geometry $\mathbf{R}(t_f)$. State-specific differential cross sections can be obtained by using the appropriate wave function $\Theta(\mathbf{x})$ for that state in the overlap Eq. (7).

The charge-transfer cross section σ_{CT} is defined as

$$\sigma_{\mathrm{CT}} = 2\pi\int_0^\infty P_{\mathrm{CT}}(b)\, b\, \mathrm{d}b, \tag{10}$$

where the probability for charge transfer, P_{CT}, is the transition probability for charge transfer defined in terms of the S matrix,

$$P_{\mathrm{CT}}(b) = |S_{i\to f}(b)|^2, \tag{11}$$

and $S_{i\to f}(b)$ is the probability amplitude for a transition from the initial state i with impact parameter b to final state f:

$$S_{i\to f}(b) = \lim_{\substack{t_i\to-\infty\\ t_f\to\infty}} \langle\Phi_{i\to f}|\Theta\rangle. \tag{12}$$

A quick way [17] to compute the overlap with the projected wave function, and thus the charge transfer cross section, is provided by the Mulliken population analysis [18].

In Sec. III, we will be interested in comparing the dynamically evolving state $|z(t),\mathbf{R}(t),\mathbf{P}(t)\rangle$ with the adiabatic or Born-Oppenheimer HF state at the same nuclear geometry. We will compare the dynamic spin orbitals $\chi_k(\mathbf{x},z(t),\mathbf{R}(t),\mathbf{P}(t))$ with the adiabatic spin orbitals $\theta_l(\mathbf{x},\mathbf{R}(t))$ by looking at the overlaps between spin orbitals,

$$O(b,t) = \left| \int \chi_k(\mathbf{x},z(t),\mathbf{R}(t),\mathbf{P}(t))\theta_l(\mathbf{x},\mathbf{R}(t))^* \mathrm{d}^3x \right|^2, \quad (13)$$

for the trajectory with impact parameter b as a function of time.

C. Details for Si^{3+}, C^{3+}, and O^{3+}

In the present study, the set of basis functions used for the atomic orbital expansion for hydrogen is the three-Gaussian Slater-type orbital (STO-3G) [$7s3p/3s1p$] basis [19] augmented with two additional s orbitals and one additional p orbital to describe the low-lying excited states of the hydrogen atom. The first s orbital and the p orbital are made as a contraction of three basis functions with exponents 0.204203, 0.0601031, and 0.0151386. The contraction coefficients for the s orbital are −0.0999672, 0.3995128, and 0.7001155. For the p orbital the contraction coefficients are 0.1559163, 0.6076837, and 0.3919574. The second s orbital consisted of a single basis function with orbital exponent 0.01. The p orbital is introduced to describe the polarizability of the hydrogen atom as well as the correct charge and induced-dipole interaction at large distance with the C^{3+}, O^{3+}, and Si^{3+} ions. The correlation-consistent polarized double-ζ (cc-pVDZ) [$12s8p/4s3p$] [20] basis set without the d orbital is used for Si^{3+}. The d orbital is not included in the basis set for Si^{3+} since its contribution to the charge-transfer process is small at lower energies. The aug-cc-pVDZ [$10s5p2d/4s3p2d$] basis set [21] is used for C^{3+} and for O^{3+}. Several test calculations were carried out by augmenting all basis sets with more diffuse orbitals, but no significant changes were observed.

Initially, the hydrogen atom and the Si^{3+}, C^{3+}, and O^{3+} projectiles are in their electronic ground states within the single-determinant approximation, i.e., HF, and using the basis sets described above. For the projectiles (Si^{3+}, C^{3+}, and O^{3+}) a range of impact parameter values b from 0.0 to 20.0 a.u. is used. Approximately 50 fully dynamic trajectories were calculated for each projectile energy. Since the electronic configuration of projectiles as well as that of the target is initially a doublet ground state, singlet and triplet total spin collision processes were analyzed. Then, a final charge-transfer cross section was obtained as the statistical average $\sigma = \frac{3}{4}\sigma_t + \frac{1}{4}\sigma_s$, where σ_t and σ_s stand for triplet and singlet cross sections, respectively.

For the O^{3+} ion, the singly occupied $2p$ orbital can be equally well oriented along the x, y, or z axes. Thus, an average on these three possible orientations is taken to calculate the final charge-transfer cross section.

III. RESULTS

In principle, a projectile can capture or lose electrons on collision with a target atom or molecule, although in the cases studied here, intuition would suggest the most likely result to be that the charged projectile captures an electron from the hydrogen atom. In the present version of ENDyne, ionization is not included. Consequently, calculations were carried out only up to projectile energies of 10 keV/amu, so that we can safely neglect the ionization channel. For the energies of interest in this work, the probability for projectile electron loss is very low and only electron transfer from the target to the projectile is expected. At the end of the calculated trajectory, the participating particles are far enough apart that they no longer interact and their properties no longer change. The final electronic wave function is obtained and the final nuclear momenta and positions are then obtained.

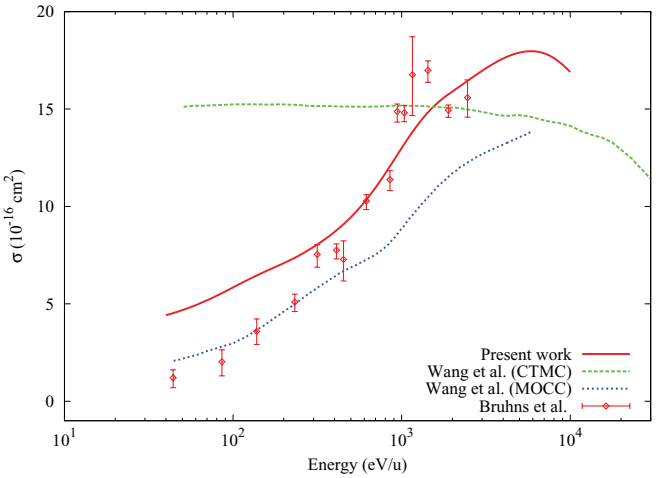

FIG. 1. (Color online) Total charge-transfer cross section for an Si^{3+} ion colliding with a hydrogen atom as a function of the projectile energy. The experimental results of Bruhns *et al.* [2] and the theoretical results of Wang *et al.* [5] using quantum-mechanical molecular-orbital close-coupling (MOCC) and classical-trajectory Monte Carlo (CTMC) methods are also shown.

A. The Si^{3+} ion

Figure 1 displays the charge transfer cross section computed in this work along with the experimental data for the Si^{3+} ion

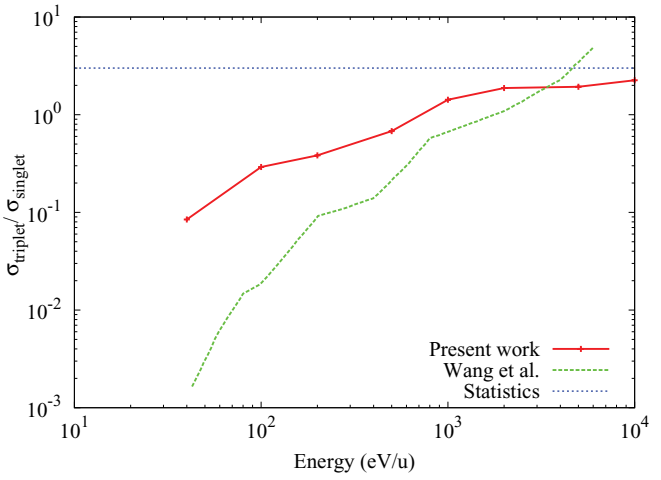

FIG. 2. (Color online) Triplet-singlet cross-section ratios for a Si^{3+} ion colliding with a hydrogen atom as a function of the projectile energy. The theoretical results of Wang *et al.* [5] (MOCC) are also shown.

colliding with hydrogen. Observe that the values of the charge-transfer cross section for the intermediate range of energy agree well with the experimental results of Bruhns *et al.* [2]. The CTMC results [5] agree neither with experimental results, as already observed by Bruhns *et al.* [2], nor with the other theoretical results in the energy range considered in the present work. Our results show a maximum at $E \approx 5$ keV/amu. At higher energies the END curve is expected to approach the CTMC cross section reported by Wang *et al.* [5] once the ionization channels, neglected in the calculation reported here, are taken into account.

Agreement with the quantal MOCC result of Wang *et al.* [5] is also good. A comparison of the present result with the quantal MOCC results shows our charge-transfer cross section result to be larger than the MOCC results by a constant difference of $2\text{–}3 \times 10^{-16}\,\text{cm}^2$ over the energy range of $0.04 < E < 1$ keV/amu. The experimental results are closer to MOCC values for lower energies and remain closer to END values for higher energies in the measured energy range. We see no obvious reason for this discrepancy. An implementation of END using fully quantum-mechanical nuclear dynamics, as used in MOCC, is in progress [22]; this may clarify whether the difference between END and MOCC results arises from the difference in the description of the nuclear or the electronic part of the problem.

The calculated ratio of triplet to singlet total charge-transfer cross section for the collision of the Si^{3+} ion with hydrogen is plotted in Fig. 2. As there are scant experimental or theoretical results available, some astrophysical models assume the final population within triplet and singlet states follows the spin statistics (i.e., 3 to 1). The ratio for the total cross section is in general agreement with the statistical value (3) at higher projectile energies, but larger differences appear for very small energies, more so for MOCC results than for END values.

In Fig. 3 we analyze the evolution of the system wave function as a function of interaction time for two representative impact parameters b at two collision energies, in terms of the projection of the dynamic END electronic wave function on the spin-unrestricted Hartree-Fock self-consistent field (SCF) determinant of spin orbitals for the nuclear geometry at that time, as discussed in Sec. II B. These spin orbitals can have different spatial parts for α and β spins. The dynamic spin orbitals in the END wave function are also spin-unrestricted. They can also have different orbital parts and evolve differently in time as well. The HF SCF orbitals used in this analysis are

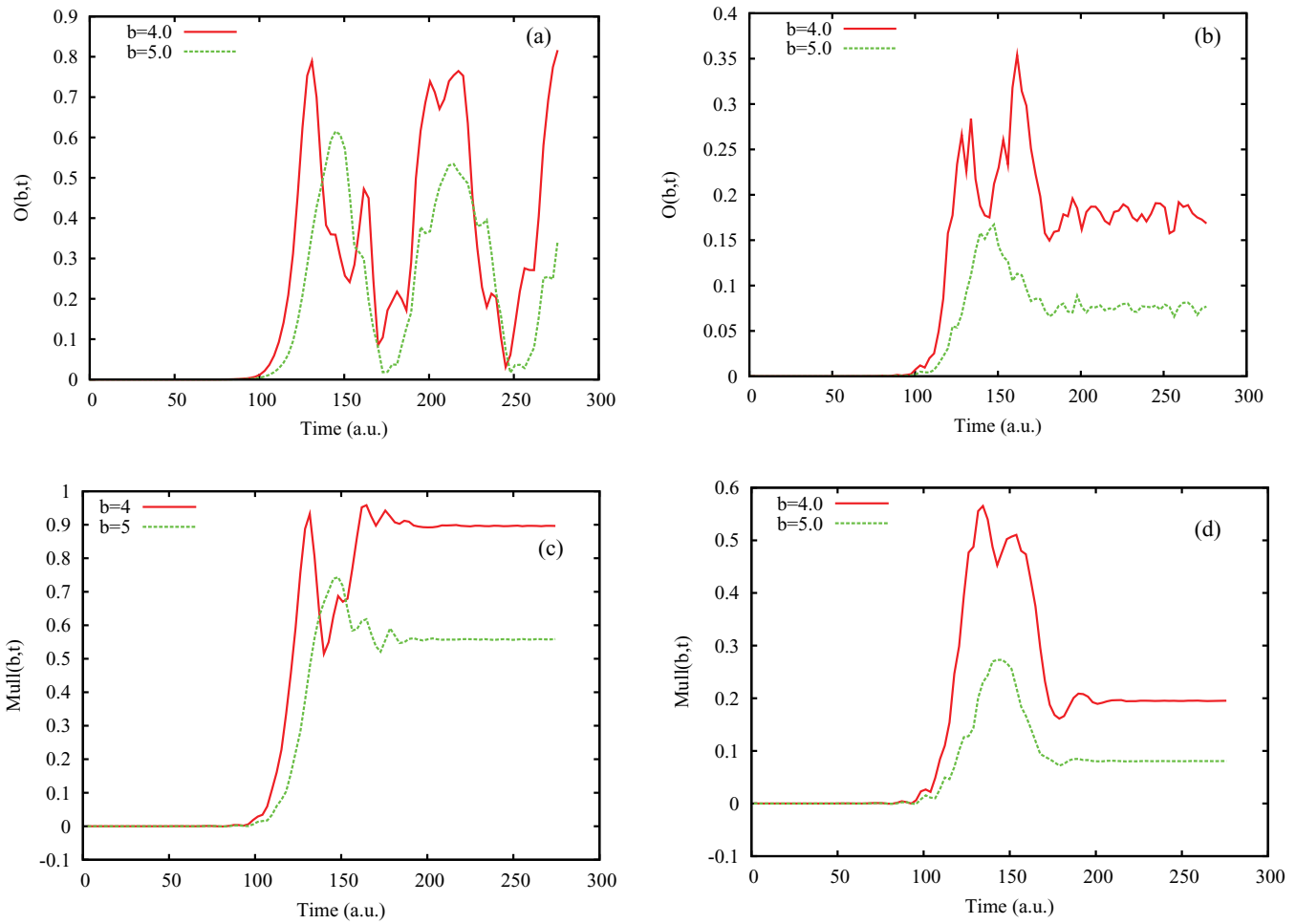

FIG. 3. (Color online) Overlap of Si^{3+} 14.5 keV END dynamic orbitals with (a) singlet and (b) triplet HF SCF $3p$ orbitals at impact parameter values $b = 4.0$ and 5.0. Panels (c) and (d) give the Mulliken population for singlet and triplet configuration, respectively. For times less than 100 a.u and larger than 300 a.u these give the transfer probability. See text for full interpretation.

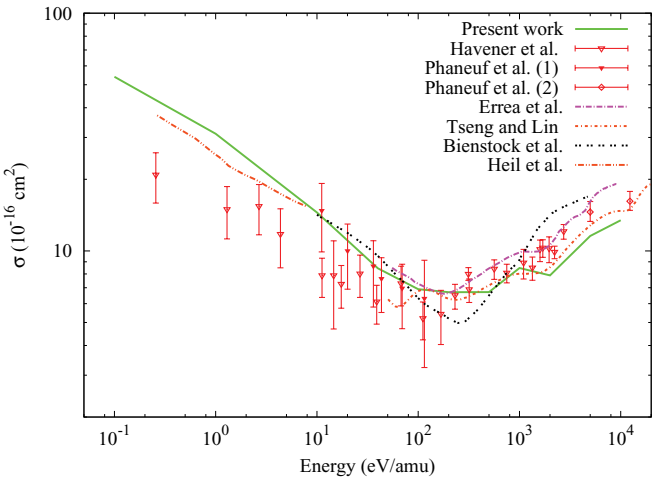

FIG. 4. (Color online) Total charge-transfer cross section for a C^{3+} ion colliding with hydrogen as a function of the projectile energy. The experimental results of Havener *et al.* [3] and Phaneuf *et al.* [24,25], and the theoretical results of Errea *et al.* [8], Tseng and Lin [7], Bienstock *et al.* [26], and Heil *et al.* [27] are also shown.

molecular orbitals of the ion-hydrogen molecule combined when the nuclei are close together and asymptotically become the $3p$ orbitals of the Si^{2+} ion. We identify these molecular SCF orbitals by the atomic orbital they continuously connect to as the internuclear distance increases. To avoid confusing information related to the orientation of the three basis orbitals, we show the sum of the amplitudes squared, which is the total fraction of the dynamic END $3p$ orbitals that lie in the SCF $3p$ subshell. Further details concerning the calculation of the overlap can be found in Ref. [23]. We also show the Mulliken population as a function of time. This gives the total electron transfer probability asymptotically for large times as the Mulliken population is known not to be meaningful for short distances, i.e., between 100 and 300 a.u. in this study. The Mulliken population becomes constant beyond the interaction region for both the singlet, Fig. 3(c), and the triplet, Fig. 3(d), indicating that the transfer is complete. A comparison of the Mulliken population at large times with the SCF projection thus gives the character of the electronic state after transfer, because the sum of the projections must add up to the total transfer probability, i.e., the Mulliken population. We do not

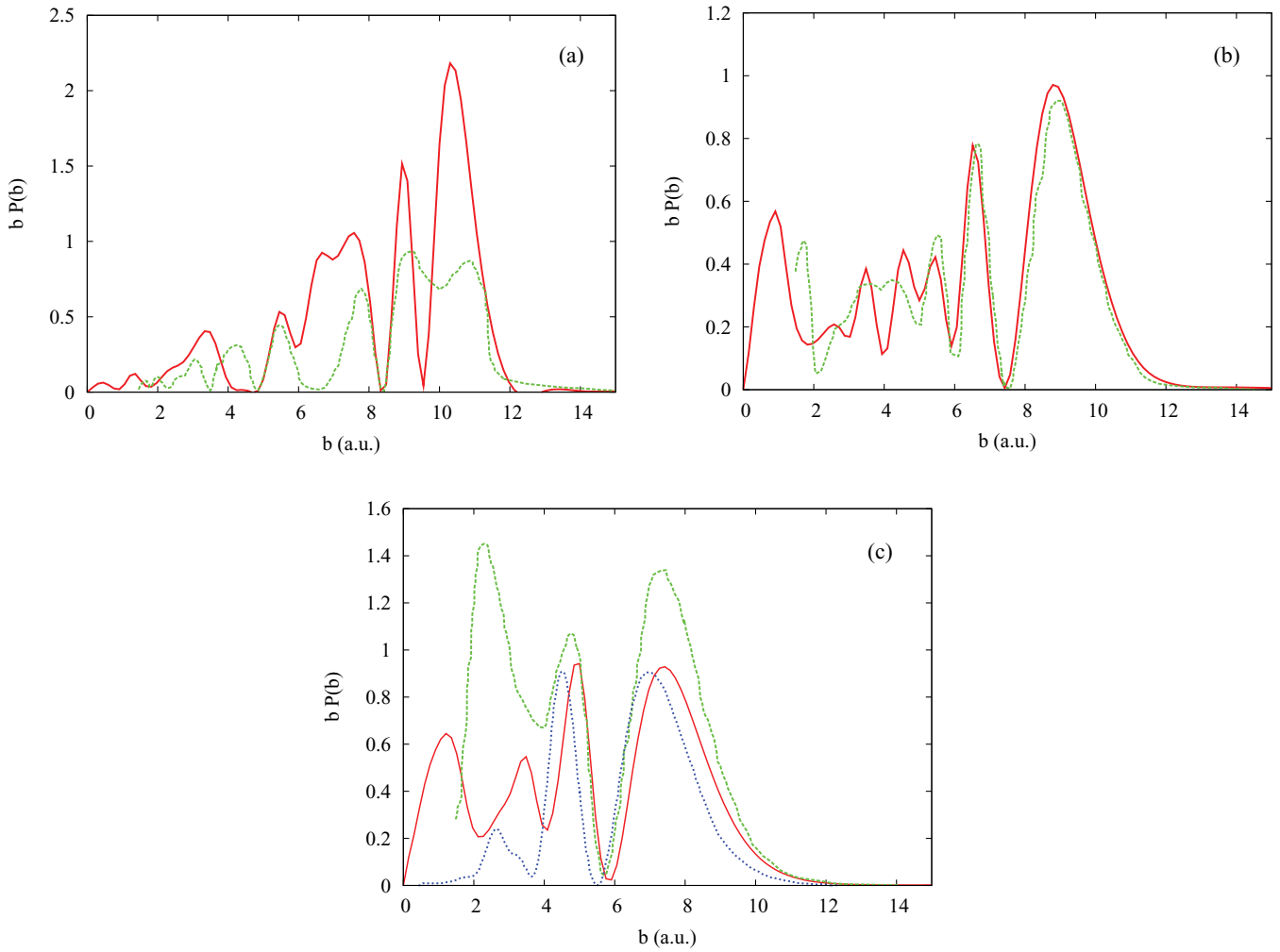

FIG. 5. (Color online) Total charge-transfer probabilities for the triplet contribution times impact parameters for a C^{3+} ion colliding with a hydrogen atom as a function of the impact parameters at projectile energies of (a) 0.05, (b) 0.5, and (c) 2 keV/amu. Results from the present work (solid line), from the calculations of Errea *et al.* [8] (dashed line), and from Tseng and Lin [7] (dotted line) are shown.

show the 1*s*, 2*s*, 2*p* core orbitals, only the set of 3*p* orbitals, because these show the most interesting behavior and are the most relevant to our analysis. The projections on other orbitals show changes as a function of time when the nuclei are in the interaction region, indicating that these orbitals are involved in the reaction process, but the projections fall back to initial values after the reactants separate.

We make the following observations with respect to Fig. 3. For the singlet, Fig. 3(a), and the triplet, Fig. 3(b), the projection on the 3*p* SCF orbitals of Si^{2+} keeps oscillating, much more so for the singlet. This indicates that the electronic state of the Si^{2+} is an excited electronic state that oscillates between the 3*s* (not shown) and the 3*p* state. The excitation is more pronounced for the singlet state. For higher energies a similar analysis has been carried with qualitatively similar results. To obtain state-specific cross sections, further projection of the evolving state is necessary. This then gives the probability that the final state is one of the stationary states of the product ion.

B. The C^{3+} ion

In Fig. 4 the total charge-transfer cross sections for the collision of C^{3+} with hydrogen along with available experimental and theoretical results are shown. Since the triplet channels are statistically favored and the charge-transfer cross section for lower energies is dominated by the triplet contribution, we extended our study to lower energies down to $E \sim 0.1$ eV/amu, and also analyzed local properties for the triplet contribution.

Our result for the charge-transfer cross section shows good agreement with the experimental data of Havener *et al.* [3] and of Phaneuf *et al.* [24,25] at intermediate to large energies. Comparison of the present result with the other theoretical data shows good agreement with Errea *et al.* [8] at intermediate energies and with Tseng and Lin [7] at larger energies. The Errea *et al.* [8] calculations are based on the molecular-orbital expansion method in the impact parameter formalism that employs classical, straight-line trajectories for the nuclei. Tseng and Lin [7] use the same semiclassical method but with an atomic orbital expansion basis.

As the projectile energy decreases for C^{3+} colliding with the atomic hydrogen, our result for the charge-transfer cross section increases in agreement with the Langevin-type cross section ($\sigma \sim E^{-1/2}$) and with the theoretical results obtained by the coupled-channel method with a quantum-mechanical description of the nuclei by Bienstock *et al.* [26] above 10 eV and by Heil *et al.* [27] for 0.27 to 8 eV. At such low energies the semiclassical treatment of the nuclear degrees of freedom in END is not reliable because the longer de Broglie wavelength will lead to interference effects between multiple trajectories. The fact that our results agree even at these low energies is an indication that nuclear quantum effects are not of primary importance in this process, or, in a semiclassical formulation, that nuclear trajectories do not exhibit strong interference effects. A fully quantum-mechanical description of the nuclei in END is being implemented [22]; this will allow us to verify and substantiate this observation in future work.

To correctly describe the Langevin-type scattering in the END treatment, we include *p* orbitals in the basis set for the hydrogen atom. This allows us to describe the charge-induced dipole interaction properly at large distance. The inclusion of

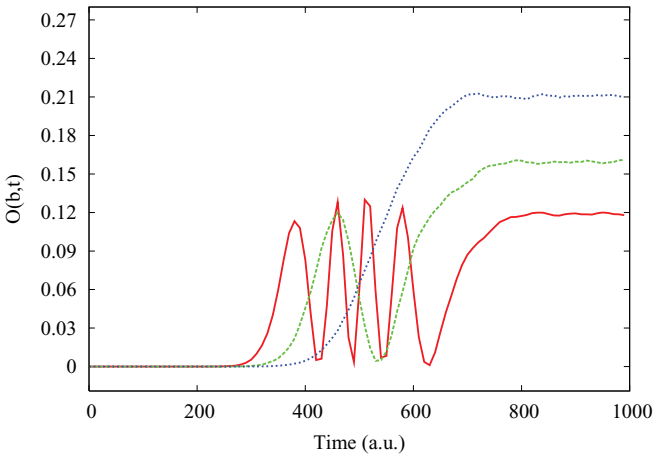

FIG. 6. (Color online) Triplet contribution to the projection of the dominant dynamic orbital in the evolving END wave function $O(b,t)$ on the 3*s* orbital of the carbon basis set along different trajectories for a C^{3+} ion colliding with hydrogen as a function of time at projectile energies of 0.05 keV/amu. Impact parameters are $b = 7$ a.u. (solid line), 9 a.u. (dashed line), and 10.5 a.u. (dotted line).

p orbitals in the basis set for the hydrogen atom generates a nonvanishing polarizability that produces a potential at large distance of the form $V \sim -1/R^4$. It is well known that the inclusion of this long-range interaction generates the Langevin-type cross section [28].

Figure 5 shows the product of the calculated total charge-transfer probabilities and the impact parameter, $bP(b)$, for the collision system for different projectile energies. We observe that the contributions from smaller impact parameters become larger at large energies. At lower energies, interference effects (Stueckelberg oscillations) become important, and contributions from large impact parameters to the charge-transfer cross section increase. Our results agree with Errea *et al.* [8] in that the charge transfer at low energies occurs mainly by

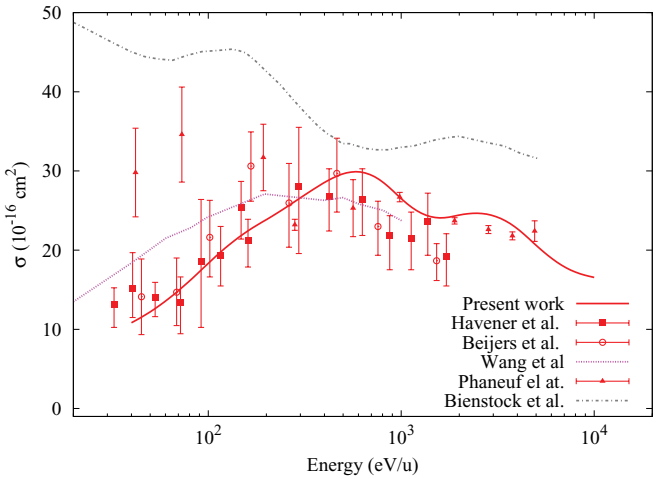

FIG. 7. (Color online) Total charge-transfer cross section for an O^{3+} ion colliding with a hydrogen atom as a function of the projectile energy. Experimental results are from Havener *et al.* [4], Beijers *et al.* [29], and Phaneuf *et al.* [25], and theoretical results using the quantal close-coupling methods are due to Wang *et al.* [6] and from Bienstock *et al.* [30].

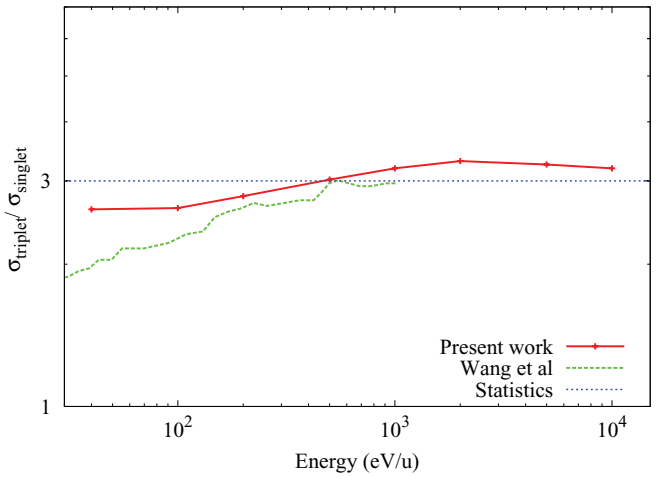

FIG. 8. (Color online) Triplet-singlet cross section ratio for an O^{3+} ion colliding with a hydrogen atom as a function of the projectile energy. The theoretical MOCC results are from Wang *et al.* [6].

electron capture into the $1s^2 2s 3s\ ^3S$ state of C^{2+}; their results are included in Fig. 5 for comparison. An analysis of the dynamic orbitals similar to that shown in Fig. 3 shows how the electron ends up in the 3*s* orbital. Figure 6 shows the overlap between the 3*s* orbital in the adiabatic HF wave function at the same geometry and the dynamic orbital in the evolving END state. We only show the overlap with the dynamic orbitals that have significant contribution for asymptotic times. We find that at asymptotic times the overlap is equal to the total transfer probability, which indicates that all of the transfer is into the $1s^2 2s 3s\ ^3S$ state.

At a projectile energy of 0.05 keV/amu, the curve structure at large impact parameters appears similar for both our calculation and the results reported by Errea, but the END probability is much larger. At $E = 0.5$ keV/amu, the structure of END results and the calculation by Errea *et al.* [8] coincide at large impact parameters. At the higher projectile energy of 2 keV/amu, the structure at large impact parameters is again similar; our results agree closely with Errea *et al.* [8] and Tseng and Lin [7]. At all energies, the curve structure at

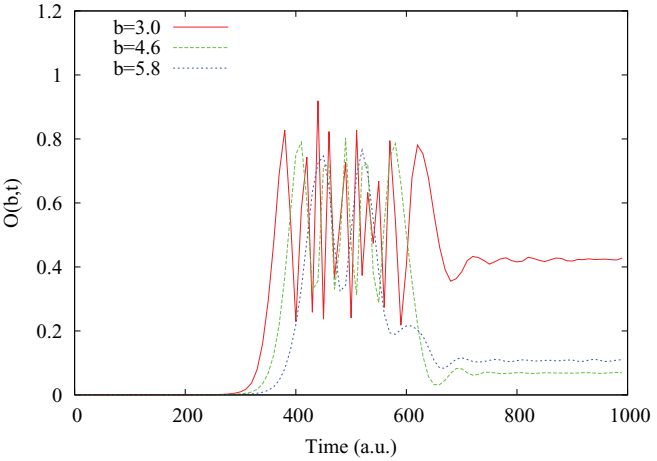

FIG. 9. (Color online) Overlap of O^{3+} 0.64 keV 3*s* END orbital singlet with the HF SCF 3*s* orbital.

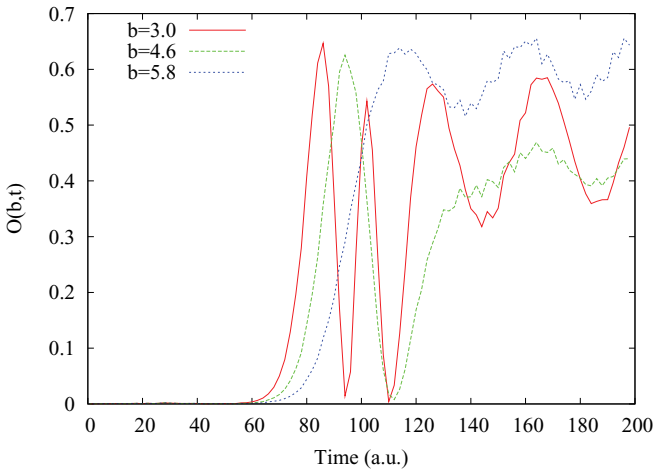

FIG. 10. (Color online) Overlap of O^{3+} 16 keV 3*s* END orbital singlet with the HF SCF 3*s* orbital.

small impact parameters does not agree with the calculations of Errea *et al.* [8]. This is to be expected since for small impact parameters the difference between straight lines [8] and dynamic trajectories computed in END will have the greatest effect.

C. The O^{3+} ion

Figure 7 shows the present calculated total charge-transfer cross sections for O^{3+} collision with a hydrogen atom along with other theoretical results and experimental data. Our result shows good agreement with the experimental data of Havener *et al.* [4] over the entire range of energies. At smaller energies our charge-transfer cross section is very close to the results of Beijers *et al.* [29], and at larger energies our calculations agree with the experimental results of Phaneuf *et al.* [25]. Better agreement is observed at larger energies with respect to the theoretical result of Wang *et al.* [6] using quantum-mechanical MOCC methods.

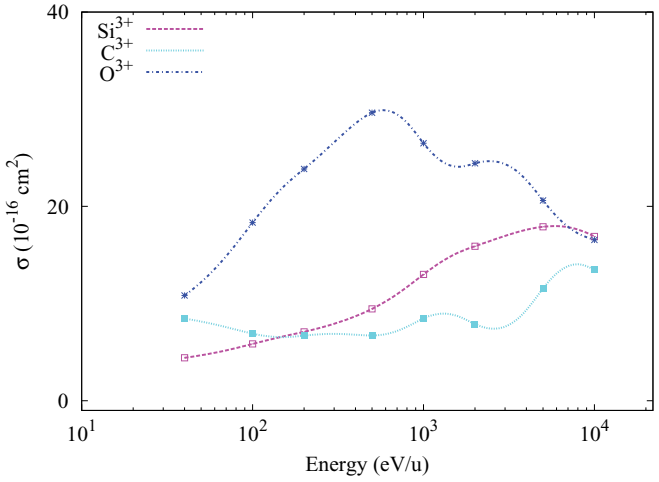

FIG. 11. (Color online) Calculated total charge-transfer cross sections for Si^{3+} (dashed line), C^{3+} (dash-dotted line), and O^{3+} (dotted line) ions colliding with a hydrogen atom as a function of the projectile energy.

The ratio of triplet to singlet charge-transfer cross sections for collision of an O^{3+} ion with a hydrogen atom is plotted in Fig. 8. At large energies, the ratio for the total cross section is in generally good agreement with the statistical value. For this collision, the ratio is closer to the statistical ratio than it is for Si^{3+} on a hydrogen atom throughout the energy range; compare with Fig. 2 in Sec. III A.

Figures 9 and 10 show the analysis of the system wave function as a function of time for the singlet state at two collision energies: 0.64 keV and 16 keV. The norm of the projection on the 3*s* HF SCF α spin orbital is shown for three impact parameters computed the same way as for the Si^{3+} ion in Sec. III A. Full analysis of the contribution from the 3*s* α spin orbital to the singlet and the triplet states shows that at low energy the transfer is predominantly into the $3s\,^3S$ and $3s\,^1P$ configurations of O^{2+}: This follows from the 3*s* projection becoming constant asymptotically and equal to the total transfer probability. For higher energy, an electronically excited state is created. This can be deduced from the fact that the projection on the 3*s* orbital keeps oscillating long after the collision is past, indicating dynamics in the electronic state of the O^{2+} product ion. Further projection on the stationary states of the O^{2+} ion then yields the result that the final state is predominantly $3s\,^3S$ and $3s\,^1P$ also at the higher energies.

IV. CONCLUSIONS

In conclusion, the total charge-transfer cross sections calculated using electron nuclear dynamics for projectile energies in the range from 0.04 to 10 keV/amu are in good agreement with experiment and with other theoretical results for the collisions of Si^{3+}, C^{3+}, and O^{3+} with atomic hydrogen. Figure 11 shows a comparison of the charge transfer cross section for the collisions of Si^{3+}, C^{3+}, and O^{3+} with atomic hydrogen at energies between 0.04 and 10 keV/amu as obtained with the END method. Each curve has been compared earlier with experimental and other theoretical results in Figs. 1, 4, and 7, respectively. Figure 11 shows the different energy dependencies of the charge-transfer cross sections for the ions pointed out by Bruhns *et al.* [2], contrary to the expectation that they all have similar behaviors because the projectiles are all effective one-electron systems with equal charges ($q = 3+$).

The Si^{3+} transfer process results in final states that have an ongoing excitation including contributions from two configurations, $1s^22s^22p^63s^2$ and $1s^22s^22p^63s3p$ character, the energy range, with the excitation being stronger for the singlet configuration. The strong changes during the collision dynamics explain why the triplet to singlet cross-section ratio in Fig. 2 is low compared to the statistical value of 3, especially at lower energies where the triplet participation remains higher, i.e., more comparable to that of the singlet.

The electron transfer to C^{3+} is a smooth process that shows less variation with energy, and results in almost complete transfer to the $1s^22s3s\,^3S$ state of C^{2+}. We see that the singlet states receive less transfer, in agreement with the earlier observations of Errea *et al.* [8] and of Bienstock *et al.* [26]. The triplet contribution to the total charge-transfer cross section is dominant and the single-determinant END approach provides reliable results for the charge-transfer cross section, including the Langevin-type cross section ($\sigma \sim E^{-1/2}$) at smaller energies, due to the proper description of the charge-induced dipole interaction at large distances.

The electron transfer to O^{3+} is the most complex, with a strong energy dependence and involving significant electronic dynamics during the collision, resulting in final states of $1s^22s^22p3s\,^3S$ and $1s^22s^22p3s\,^1P$ in the statistical triplet to singlet ratio of 3 to 1. The large effect is understandable from the observation that the valence electron for O^{3+} is not a lone electron outside a filled shell, as is the case for C^{3+} and Si^{3+}, but is in a subshell (2*p* orbital), where interaction with other electrons in the same shell (i.e., the 2*s* electrons) can be important.

ACKNOWLEDGMENTS

This work was completed with support of NSF Grant No. CHE-0513386 to N.Y.Ö. and E.D. We acknowledge the support of the University of Florida High Performance Computing center for computational resources. The authors would like to thank Prof. R. Longo for useful comments and the anonymous referee for important suggestions that significantly improved the presentation of the paper.

[1] G. Steigman, Astrophys. J. **199**, 642 (1975).
[2] H. Bruhns, H. Kreckel, D. W. Savin, D. G. Seely, and C. C. Havener, Phys. Rev. A **77**, 064702 (2008).
[3] C. C. Havener, A. Müller, P. A. Zeijlmans van Emmichoven, and R. A. Phaneuf, Phys. Rev. A **51**, 2982 (1995).
[4] C. C. Havener, M. P. Nesnidal, M. R. Porter, and R. A. Phaneuf, Nucl. Instrum. Methods Phys. Res., Sect. B **56-57**, 95 (1991).
[5] J. G. Wang, B. He, Y. Ning, C. L. Liu, J. Yan, P. C. Stancil, and D. R. Schultz, Phys. Rev. A **74**, 052709 (2006).
[6] J. G. Wang, P. C. Stancil, A. R. Turner, and D. L. Cooper, Phys. Rev. A **67**, 012710 (2003).
[7] H. C. Tseng and C. D. Lin, J. Phys. B **32**, 5271 (1999).
[8] L. F. Errea, B. Herrero, L. Méndez, and A. Riera, J. Phys. B **24**, 4061 (1991).
[9] E. Deumens, A. Diz, H. Taylor, and Y. Öhrn, J. Chem. Phys. **96**, 6820 (1992).
[10] E. Deumens, A. Diz, R. Longo, and Y. Öhrn, Rev. Mod. Phys. **66**, 917 (1994).
[11] R. Longo, A. Diz, E. Deumens, and N. Y. Öhrn, Chem. Phys. Lett. **220**, 305 (1994).
[12] P. Kramer and M. Saraceno, *Geometry of the Time-Dependent Variational Principle in Quantum Mechanics* (Springer-Verlag, New York, 1981).
[13] J. R. Klauder and B. S. Skagerstman, *Coherent States, Applications in Physics and Mathematical Physics* (World Scientific, Singapore, 1985).
[14] D. J. Thouless, Nucl. Phys. **21**, 225 (1960).
[15] J. B. Delos, Rev. Mod. Phys. **53**, 287 (1981).

[16] E. Deumens, T. Helgaker, A. Diz, H. Taylor, J. Oreiro, B. Mogensen, J. A. Morales, M. C. Neto, R. Cabrera-Trujillo, and D. Jacquemin, ENDYNE version 2.8 Sofware for Electron Nuclear Dynamic, Quantum Theory Project, University of Florida, Gainesville, FL 32611-8435 (2000).
[17] R. Cabrera-Trujillo, J. R. Sabin, Y. Öhrn, and E. Deumens, Phys. Rev. A **61**, 032719 (2000).
[18] R. S. Mulliken, J. Chem. Phys. **36**, 3428 (1962).
[19] W. J. Hehre, R. F. Stewart, and J. A. Pople, J. Chem. Phys. **51**, 2657 (1969).
[20] D. E. Woon and T. H. Dunning Jr., J. Chem. Phys. **98**, 1358 (1993).
[21] T. H. Dunning Jr., J. Chem. Phys. **90**, 1007 (1989).
[22] B. Hall, Ph.D. thesis, in progress (2011).
[23] N. L. Guevara, E. Teixeira, B. Hall, E. Deumens, Y. Öhrn, and J. R. Sabin, Phys. Rev. A **80**, 062715 (2009)
[24] R. A. Phaneuf, F. W. Meyer, and R. H. McKnight, Phys. Rev. A **17**, 534 (1978).
[25] R. A. Phaneuf, I. Alvarez, F. W. Meyer, and D. H. Crandall, Phys. Rev. A **26**, 1892 (1982).
[26] S. Bienstock, T. G. Heil, C. Bottcher, and A. Dalgarno, Phys. Rev. A **25**, 2850 (1982).
[27] T. G. Heil, S. E. Butler, and A. Dalgarno, Phys. Rev. A **23**, 1100 (1981).
[28] C. A. Feickert, R. J. Blint, G. T. Surrat, and W. D. Watson, Astrophys. J. **286**, 371 (1984).
[29] J. P. M. Beijers, R. Hoekstra, and R. Morgenstern, J. Phys. B **29**, 1397 (1996).
[30] S. Bienstock, T. G. Heil, and A. Dalgarno, Phys. Rev. A **27**, 2741 (1983).